






Tunable spin-glass optical simulator based on multiple light scatteringGianni Jacucci ^{1,*},[†] Louis Delloye ^{1,*} Davide Pierangeli,^{2,3} Mushegh Rafayelyan ⁴,
Claudio Conti ^{2,3} and Sylvain Gigan ¹¹*Laboratoire Kastler Brossel, Sorbonne Université, Ecole Normale Supérieure-Paris Sciences et Lettres Research University, Centre Nationale de la Recherche Scientifique, UMR 8552, Collège de France, 24 rue Lhomond, 75005 Paris, France*²*Institute for Complex Systems, National Research Council, 00185 Rome, Italy*³*Dipartimento di Fisica, Università di Roma “La Sapienza,” 00185 Rome, Italy*⁴*Department of Physics, Yerevan State University, 0025 Yerevan, Armenia*

(Received 12 November 2021; revised 7 February 2022; accepted 17 February 2022; published 3 March 2022)

The race to heuristically solve nondeterministic polynomial-time (NP) problems through efficient methods is ongoing. Recently, optics was demonstrated as a promising tool to find the ground state of a spin-glass Ising Hamiltonian, which represents an archetypal NP problem. However, achieving completely programmable spin couplings in these large-scale optical Ising simulators remains an open challenge. Here, by exploiting the knowledge of the transmission matrix of a random medium, we experimentally demonstrate the possibility of controlling the couplings of a fully connected Ising spin system. By tailoring the input wave front we showcase the possibility of modifying the Ising Hamiltonian both by accounting for an external magnetic field and by controlling the number of degenerate ground states and their properties and probabilities. Our results represent a relevant step toward the realization of fully programmable Ising machines on thin optical-platforms that are capable of solving complex spin-glass Hamiltonians on a large scale.

DOI: [10.1103/PhysRevA.105.033502](https://doi.org/10.1103/PhysRevA.105.033502)**I. INTRODUCTION**

Nondeterministic polynomial-time problems, also known as NP problems, are tasks whose solve time scales exponentially with the size of the input [1]. Such problems appear in most domains, including the economy, society, science, and cryptography [2]. Importantly, NP-complete problems can be mapped onto each other, and solving one solves them all. Among these, finding the ground state of an Ising spin system represents one of the most well known examples in physics [3–7].

Interestingly, Ising dynamics have been observed in numerous quantum [8,9] and classical systems such as random lasers [10,11], superconducting networks [12,13], polariton condensates [14,15], nonlinear wave propagation in disordered media [16], and degenerate optical parametric oscillators [17–29]. Therefore, all aforementioned systems represent suitable platforms to implement NP problem solvers. For example, coherent Ising machines using degenerate optical parametric oscillators find approximate solutions for the ground state of spin systems, thanks to their inherent nonlinearity, with great control of their couplings. Although optical parametric oscillators can now implement thousands of spins [24], their scalability remains limited by electronic circuits.

Recently, a second class of optical simulators based on linear optics was demonstrated by exploiting spatial light modulation [30–36]. In these Ising machines—where the spins and their interactions are described by phase and am-

plitude modulation [30–34] or by a properly engineered gauge transformation on the optical wave front [35,36]—the ground state is found by optimizing the detected intensity via a recurrent electro-optical feedback. The advantage of this approach relies on the instantaneous calculation of the energy, as the necessary matrix products are encoded in light propagation and are therefore independent of the number of spins.

However, photonic Ising machines based on wave-front shaping using free-space propagation are limited to the implementation of a specific class of Hamiltonians, known as Mattis models [37], where the couplings between spins are correlated and an exact solution of the energy ground state exists. Recently, a more general class of Hamiltonians, known as Sherrington-Kirkpatrick spin glasses [38,39], in which the couplings are all to all and random, was simulated by combining wave-front shaping and light propagation inside a random medium [32,34]. Although this optical simulator is scalable and can outperform conventional hardware for a large number of spins [32], its applicability was limited to random all-to-all couplings with zero average, as determined by the transmission matrix of a random medium.

In this article, we present various strategies to tune the couplings of a spin-glass Ising simulator based on multiple light scattering. We experimentally demonstrate the ability to control the evolution of a system in a deterministic fashion by exploiting the knowledge of the transmission matrix of the scattering medium [40]. This allows us to observe the phase transition from a disordered to a fully magnetized ground state. Moreover, our work showcases the possibility of modifying the simulated Ising Hamiltonian by both introducing an external magnetic-field term and controlling the number of degenerate ground states.

*These authors contributed equally to this work.

[†]Corresponding author: giovanni.iacucci@lkb.ens.fr

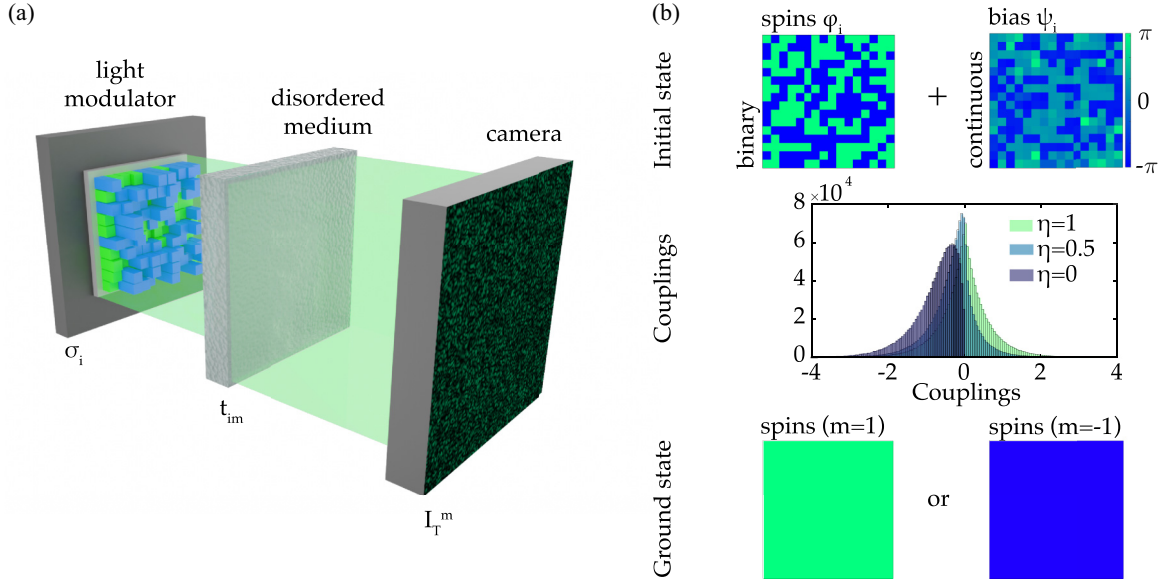


FIG. 1. Concept of a tunable optical Ising simulator. (a) Schematics of the Ising machine based on multiple scattering. The spins are encoded in a binary phase on the spatial light modulator. The ground state of the Ising Hamiltonian corresponds to the optimized binary phase mask maximizing the transmitted intensity recorded by a camera. The all-to-all, random couplings of the spins are induced by multiple light scattering during the propagation in the disordered medium, described by the transmission matrix T . (b) Measuring T determines the correct bias ψ_i to add to the initial phase mask to tune the distribution of couplings. In the case of fully biased couplings ($\eta = 0$), the final state corresponds to a fully magnetized degenerate ground state.

II. RESULTS

A system of N spins is described by the following Hamiltonian [38,39]:

$$H = - \sum_{i,j=1}^N J_{ij} \sigma_i \sigma_j, \quad (1)$$

where $\sigma_{\{i,j\}}$ and J_{ij} are the spins and their couplings, respectively. For all-to-all random couplings, J_{ij} have independent, identically distributed (i.i.d) random values, and finding the ground state of Eq. (1), which is referred to as the Sherrington-Kirkpatrick model [5], represents an NP-hard problem. This specific problem can be mapped into light propagation in disordered media, where the spins are encoded on a set of input modes or pixels with a binary phase state of 0 and π , corresponding to ± 1 spin states, respectively [32,34]. This equivalence can be made explicit by writing the transmitted intensity after a multiple scattering medium as [32]

$$I_r = \sum_{i,j=1}^N J_{ij} \sigma_i \sigma_j = -H, \quad (2)$$

with $J_{ij} = - \sum_m^M \text{Re}\{\overline{t_{im}} t_{jm}\}$, where m runs on the output modes and t_{im} and t_{jm} are transmission matrix T elements. T is linked to the input modes on the spatial light modulator (SLM) E_{in} and the output modes on the camera E_{out} via $E_{out} = T E_{in}$ [40].

Equation (2) shows that maximizing the light intensity over the selected output modes allows us to retrieve the ground state of the spin system (details on the numerical framework used can be found in Appendix B) [32]. In particular, as the distribution of couplings is Gaussian and centered around

zero, the ground state corresponds to an ensemble of randomly oriented spins (mean magnetization $m = \sum_i^N \sigma_i = 0$).

As shown in Fig. 1(b), the J_{ij} distribution can be modified by acting on the initial phases on the SLM. Indeed, such an operation leads to the following effective transmission matrix T' :

$$T' = T \times \text{diag}(e^{i\psi_i}), \quad (3)$$

where ψ_i represents the bias associated with each spin. Equation (3) rewritten in terms of matrix coefficients becomes

$$t'_{im} = t_{im} e^{i\psi_i}, \quad (4)$$

therefore, the resulting couplings, for simplicity still indicated as J_{ij} , where $J_{ij} = - \sum_m^M \text{Re}\{t'_{im} \overline{t'_{jm}}\}$, can be modified by tailoring the bias.

An efficient way to tune the couplings is to exploit the knowledge of T . In particular, for a single output mode ($M = 1$), using as ψ_i the phase conjugation of the corresponding single-row T [$\psi_i = -\arg(t_i)$] gives rise to a J_{ij} distribution of only negative values. This results from the fact that after phase conjugation T' is real valued. Figure 1(b) shows also that, consistent with having a negative average coupling $\langle J_{ij} \rangle$, the ground state of the spin network is no longer random, and it exhibits a fully magnetized state with degenerate orientations ($m = \pm 1$).

This result can also be understood in the framework of wave-front shaping [41]. The introduced bias is the phase mask that optimizes the detected intensity, of which the binary spin mask represents an undesired perturbation. Therefore, the optimal intensity is retrieved when the spin mask is reduced to a uniform phase, which in terms of spins corresponds to a fully magnetized ground state.

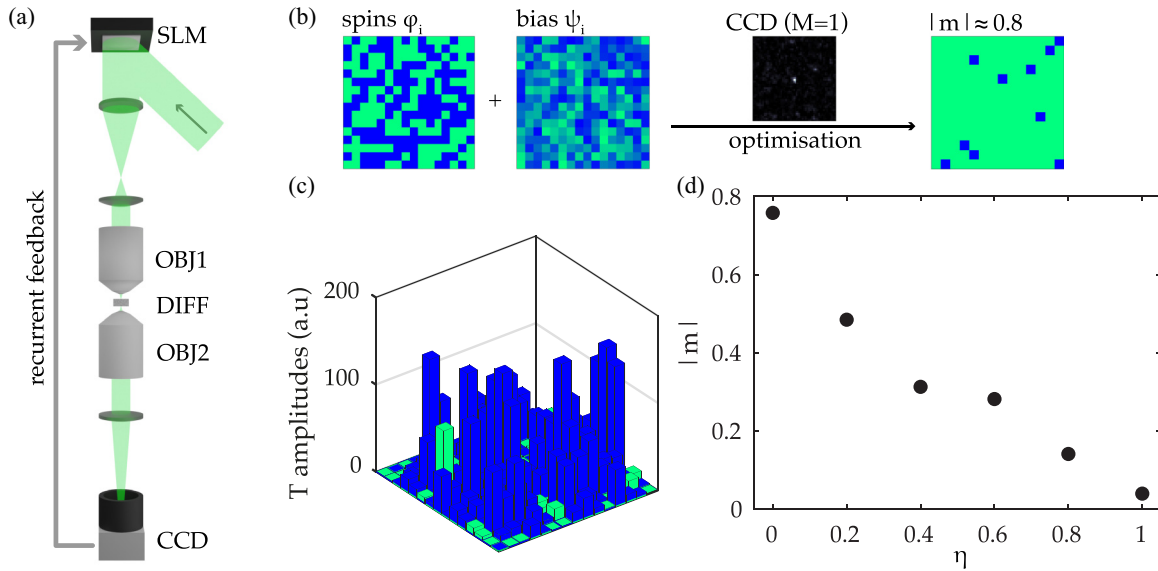


FIG. 2. Tunable experimental spin-glass simulator ($M = 1$). (a) Schematics of the experimental setup. Recurrent feedback from the measured intensity on a CCD updates the SLM configuration to reach the spin glass (SG) ground state. (b) Adding a bias to the spin system ($N = 256$ spins) results in a more magnetized ground state. Inset: intensity focus on the CCD plane as the ground state is reached. (c) The relatively low magnetization compared to the simulation value can be understood in terms of the finite detection sensibility of the CCD. The spins which are not aligned with the dominant orientation [green (light gray) bars] are indeed those whose T amplitudes, and therefore intensity contributions, are the lowest. (d) The degree of magnetization of the ground state can be readily tuned by adding artificial noise—a mask of random phases of amplitude η —to the bias.

The shift of J_{ij} can be further controlled by adding a noise mask (mask of random phases) to the phase-conjugation solution. This noise mask is modulated by an amplitude parameter η controlling the shift of the couplings, as shown in Fig. 1(b). A derivation of the effect of noise on the couplings is presented in Appendix C.

We tested experimentally our approach for controlling the couplings of the spin simulator [Fig. 2(a) and Appendix A]. A laser (Coherent Sapphire SF 532, $\lambda = 532$ nm) is directed onto a reflective phase-only, liquid-crystal SLM (Meadowlark Optics HSP192-532, 1920×1152 pixels) divided into N macropixels (spins). The modulated light is projected on the objective back focal plane (OBJ1, $10\times$, $NA = 0.1$) and focused on a scattering medium made of Teflon (DIFF) 0.5 mm thick. The scattered light is collected by a second objective (OBJ2, $20\times$, numerical aperture $NA = 0.4$), and the transmitted intensity is detected by a CCD camera (Basler aca2040-55 μm , 2048×1536 pixels). The spins and the desired bias are encoded by a SLM in a phase pattern whose binary part is sequentially updated until the ground state is reached. Note that for the optimization any algorithm can be used; that is, the setup is algorithm agnostic, as the advantage of the presented simulators resides in the parallel measurements of the energy [32].

Figure 2(b) shows the results for a single output mode ($M = 1$) on the detection camera (CCD). The ground state agrees with the numerical predictions in Fig. 1(b), showing a high magnetization. Figure 1(b) shows a typical ground state averaged over thermal fluctuations [31] [see Fig. 5(a) for single realizations].

The difference in numerical [see Fig. 1(b), $|m| = 1$] and experimental [see Fig. 2(b), $|m| \simeq 0.8$] results can be explained by the contributions that each SLM pixel bears. Indeed, as shown in Fig. 2(c), the spins not aligned with the dominant orientation correspond to SLM pixels with very small T amplitudes; that is, they marginally contribute to the output intensity and therefore cannot be detected over the optimization. The limited sensitivity of the detection camera introduces an experimental noise term, which allows the spins with small T amplitudes to have any possible orientation. It is equivalent to state that the experimental Ising simulator has an effective, finite temperature [32]. Figure 2(c) is corroborated by Fig. 5(b), showing that the light intensity retrieved after optimization is close to that obtained from phase conjugation even if the magnetization does not reach its theoretical maximum.

Moreover, building upon T , it is possible to drive the optical spin system over a phase transition. By adding artificial noise, controlled by the amplitude η (see Appendix C), to the phase-conjugated mask enables us to control the degree of magnetization reached in the ground state [see Fig. 2(d)]. This can also be understood in terms of couplings: as predicted in Fig. 1(b), introducing artificial noise effectively tunes the J_{ij} distribution.

Figure 2 summarizes the case of $M = 1$, which simplifies Eq. (1) to the class of the Mattis Hamiltonian in which J_{ij} are correlated [32,34,37]. However, such systems are described by an Ising simulator in which light propagates in free space [30,31,35,36]. Taking advantage of the all-to-all random couplings introduced by the scattering medium is necessary to focus on a higher number of output modes ($M > 1$). Maximizing the optical intensity on an area of multiple pixels represents a more complex wave-front-shaping task because

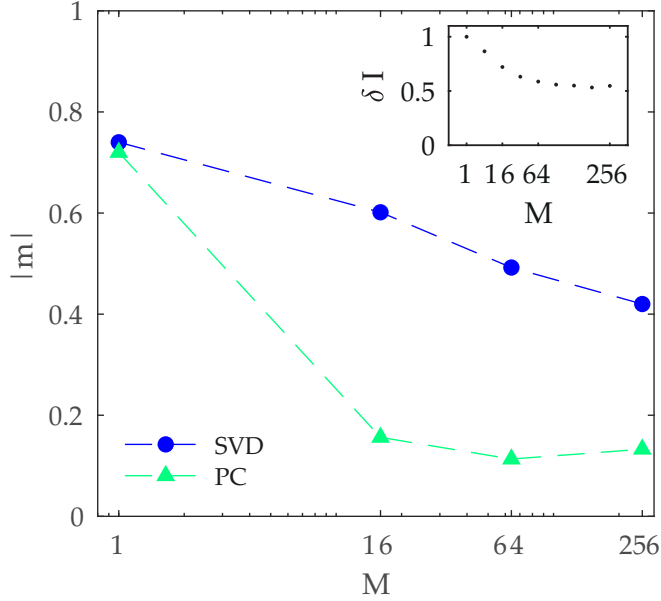


FIG. 3. Tunable experimental spin-glass simulator ($M > 1$). Magnetization as a function of the number of output modes M on the CCD. Using the first singular value decomposition (SVD) of T yields a magnetization notably larger than that with phase conjugation (PC). This can be understood by comparing the relative focus intensity δI of the two methods: numerical simulations show that the SVD outperforms the PC when M is increased, with a twofold enhancement for a square T ($N = M = 256$). The inset displays the intensity distribution on the CCD for the two approaches—for a square T the SVD yields a less homogeneous intensity distribution compared to PC.

T now has a size of $M \times N$ and the number of accessible input is N . The corresponding spin couplings satisfy $\text{rank}(J_{ij}) = N$, which implies a NP optimization problem for the ground-state search [32].

In the following, we exploit two approaches to choose the optimal bias for $M > 1$ modes: (i) carrying out the phase conjugation (PC) of the sum of the T rows and (ii) performing the singular value decomposition (SVD) of T and using the argument of the first right singular vector, i.e., the vector associated with the largest singular value [42–44]. More details on approaches (i) and (ii) are given in Appendix A. The SVD results are more effective in inducing a magnetization as the size of T increases [see Figs. 3 and 6(a) for experimental and numerical results, respectively].

Indeed, the SVD mask leads to a higher focus enhancement than the PC one, with a twofold enhancement for a square T ($N = M = 256$), and it produces a more marked shift of the J_{ij} distribution (see the inset in Fig. 3 and also Fig. 7).

A decrease of the magnetization as a function of M can again be understood in terms of T amplitudes. Figure 6(b) shows that for $M = 256$ a correlation between the alignment of the spins and their T amplitudes is observed. However, compared to $M = 1$ (see Fig. 2), the T amplitudes are more homogeneously distributed and decrease in value, meaning that more spins make a marginal, experimentally undetectable contribution to the intensity.

In Figs. 2 and 3 we demonstrate that, by measuring T , a magnetized ground state can be promoted in a spin system with all-to-all couplings. Importantly, the presented approach can also be used to generalize Eq. (1), accounting for an external magnetic field. In particular, as derived in Appendix C, by selecting a given portion of the SLM to stay fixed to a specific phase (β) defined before the optimization, i.e., by defining m SLM modes with phases $b_1, b_2, \dots, b_N = b$, Eq. (2) becomes

$$I_T = \sum_{i,j=1}^N J_{ij} \sigma_i \sigma_j + B \sum_i \sigma_i, \quad (5)$$

where $B \propto \text{Re}\{e^{i\beta}\}$ represents the added external field, defined from a fixed phase, $\beta \in [0, 2\pi)$.

This term represents a constant external magnetic field, driving the spins towards a specific sign of magnetization. In the two limiting cases $\beta = 0, \pi$ the machine is expected to settle a nondegenerate ground state that depends on the value of β [see Fig. 4(a)]. Note that the bias is applied also to the area of the SLM dedicated to the external field to effectively drive the evolution of the spins. Moreover, β tunes the intensity of the magnetic field and therefore the transition between the two degenerate spins' orientations [see Fig. 4(b)]. The sharpness of this transition is defined by the ratio between the number of SLM pixels allocated to the spins and those describing the magnetic field (see Fig. 8).

Remarkably, the ground state found by the spin-glass simulator can be further modified by adding a tailored, binary shift to the T bias γ . With this modification, the system will converge to the defined shift pattern [see Fig. 4(c)]. Figure 4(c) shows that a ground state resembling an antiferromagnetic system is obtained by defining $\gamma_k = (1 - e^{i\pi k})\Gamma$, with $\Gamma \in [0, 2\pi]$. The fidelity of the ground state, quantified in terms of staggered magnetization m' [45], is close to what was observed in Fig. 1(b). Moreover, Fig. 4(d) shows that by varying the angle associated with the additional shift mask Γ , the energy landscape of the system can be affected. Without any additional shift, the ground state is fully magnetized, as already shown in Fig. 1(b). When $\Gamma = \frac{\pi}{2}$, the system has an additional equiprobable ground state which becomes dominant when $\Gamma = \pi$. The form this shift and corresponding ground state take can be extended to any arbitrary mask (Fig. 9).

III. CONCLUSION

In conclusion, we reported an approach to tailor the Hamiltonian of all-to-all coupled spin systems implemented on a spatial photonic Ising machine. In contrast to previous works, our method controls the couplings by shifting their distribution. Such tunability was obtained by exploiting the complex coefficients of the transmission matrix and tuning the number of output modes. In particular, knowing the transmission matrix allows us to map a Sherrington-Kirkpatrick spin-glass model with tunable couplings and an external field term through a copropagating reference on the input wave front. Finally, we demonstrated that greater control over the energy landscape—and hence the possible ground states and their likelihood—can be obtained by introducing a tailored binary phase shift.

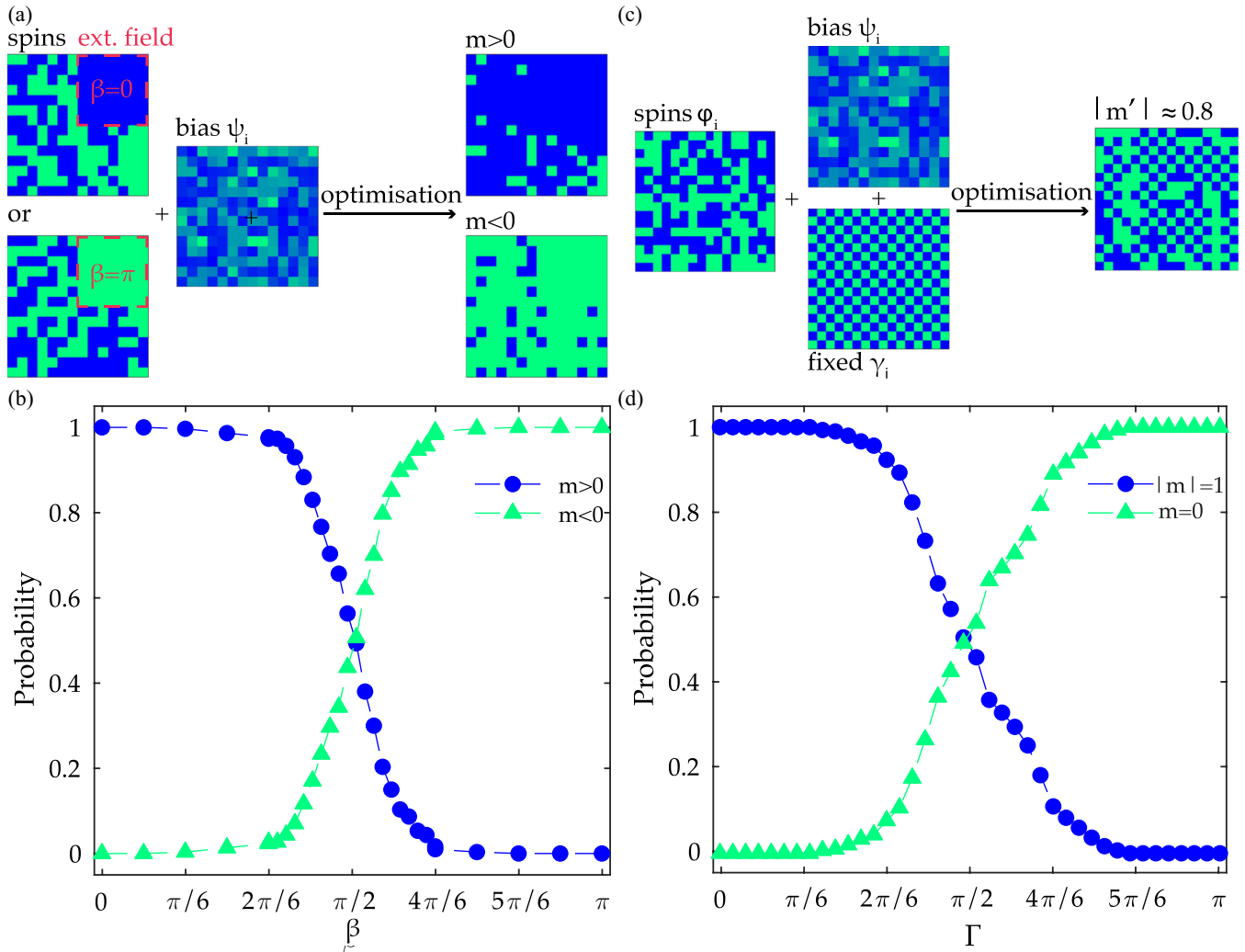


FIG. 4. Modifying the Hamiltonian of an Ising simulator to control the ground state of a spin system. (a) A constant external magnetic field is implemented by fixing a section of the SLM. The angle associated with the fixed area β determines the final state of the spin system. (b) Tuning β allows transitioning between the two magnetized states with opposite orientations. (c) Adding a binary pattern γ_i to the bias is possible to determine the spatial distribution of the spins in the ground state. In particular, by using a checkerboard with binary values of 0 and π results in an antiferromagneticlike ground state, whose fidelity to the bias was quantified in terms of staggered magnetization $|m'|$. (d) Changing the value of Γ in the checkerboard part controls the probability of obtaining a ferromagnetic ($|m| = 1$) or an antiferromagneticlike ($m = 0$) ground state. Remarkably, when $\Gamma = \pi/2$, the Ising Hamiltonian presents three ground states, with a degenerate probability for the ferro- and antiferromagnetic states.

The accuracy of the Ising machine, quantified in terms of magnetization and transmission matrix amplitudes, can be improved by reducing the experimental noise of the setup. However, to target specific couplings a different approach is required. In particular, we foresee two possible routes: (i) developing algorithms that take advantage of the huge number of pixels of both the SLM and the camera to choose or group them to redefine a spin system with the target couplings and (ii) replacing the random medium with an engineered system that maps the desired couplings. Although computationally and experimentally challenging, these strategies may unlock the ability to have a fully tunable spin-glass Hamiltonian. Moreover, the performance of the Ising machine could be further improved by replacing the electro-optical feedback in the ground-state search with an all-optical, wave-front-shaping approach [46]

ACKNOWLEDGMENTS

We thank Dr. R. Pandya and Dr. J. Dong for useful discussions. This project was funded by the European Research Council under Grant Agreement No. 724473 (SMARTIES). D.P. and C.C. acknowledge funding from a SAPIExcellence BE-FOR-ERC 2020 grant, the QuantERA European Research Area Network (ERA-NET) Cofund [Grant No. 731473, the “Quantum Information Processing with Complex Media” (QuompleX) project], the Progetti di Ricerca di Interesse Nazionale (PRIN) 2017 program (Photonic Extreme Learning Machine–PELM project). M.R. acknowledges funding from the Science Committee of Armenia under Grant Agreements No. 20TTSG-1C008 and No. 21APP-1C016.

G.J., L.D., D.P., M.R., C.C., and S.G. designed the project. L.D. and G.J. carried out experiments, numerical simulations,

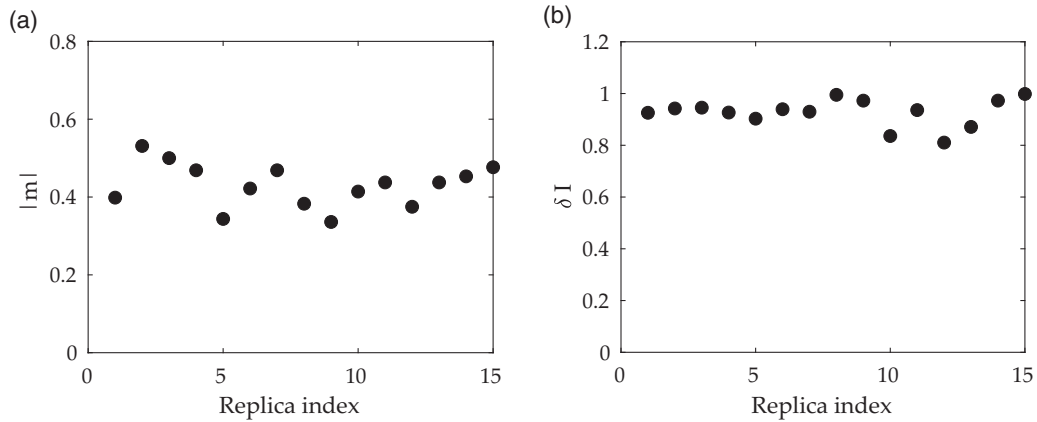


FIG. 5. (a) Magnetization values of different experimental realizations. Averaging the spins' optimal mask allows us to account for thermal fluctuations and obtain a reliable ground state [as shown in Fig. 1(b) in the main text] to compare to the corresponding theoretical zero-temperature solution. A noise-driven annealing approach does not improve the performance of the optimization. (b) Comparison between the focus intensity obtained via optimization and from phase conjugation of the TM for $M = 1$. The relative focus intensity δI is close to unity, showing that the optimization correctly reaches the highest focus intensity.

and data analysis. G.J. and L.D. wrote the paper with contributions from all the authors.

APPENDIX A: EXPERIMENTAL DETAILS

1. Transmission matrix calculation and ground-state search

The transmission matrix (TM) of the scattering medium was estimated as in [40]. In detail, each row of the TM can be reconstructed by monitoring how the intensity on a given CCD pixel changes when a phase modulation is applied to the input patterns on the SLM. The TM is sensitive to translations and rotations of the scattering medium as well as to the input and detection hardware. In this work, we define the stability as a variation within 10% of its original value. The time is long enough to run our experiments, but for larger systems one would need more stable architectures.

The ground-state search is conducted sequentially by means of the recurrent digital feedback. Computation starts from a random configuration of N binary macropixels (spins) on the SLM. The measured intensity distribution determines the feedback signal. At iteration, an arbitrary batch of spins is randomly flipped if it increases the intensity at a chosen output mode. The batch size decreases over the optimization procedure, going from 12% of the pixels to a single pixel for the last ~ 600 iterations. Note that our simulator is agnostic to the optimization algorithm used.

2. Focusing on multiple output modes: Phase conjugation and singular value decomposition

The ideal option to perfectly focus through a medium would be to be able to invert the transmission matrix. But this is extremely hard to do; in practice we use only the phase-conjugated matrix. Each element of this matrix is defined as a

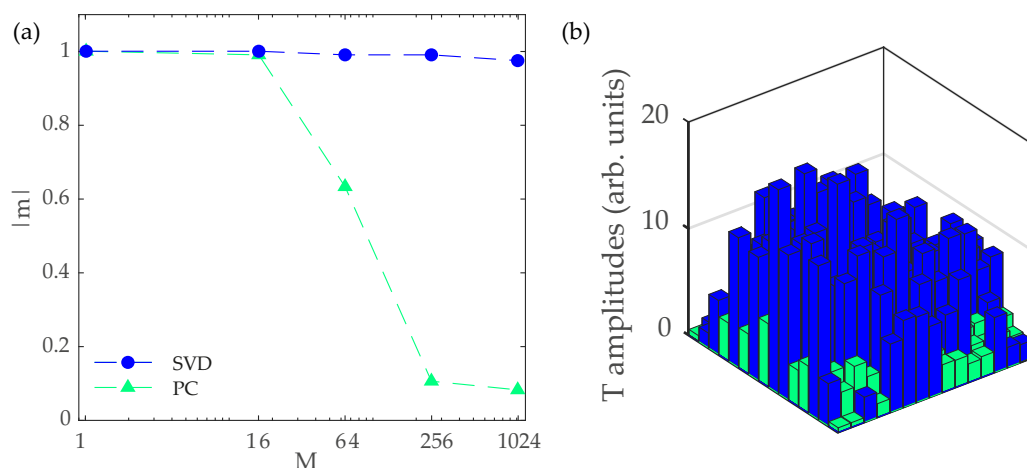


FIG. 6. (a) Simulation of the expected magnetization as a function of the number of output modes for both SVD and PC biases. (b) TM amplitudes associated with the SLM spins when considering $M = 256$. As in Fig. 2, a correlation between the alignment of the spins and their TM amplitudes is observed. Compared to $M = 1$, the TM amplitudes are more homogeneously distributed and significantly decrease in value, leading to a lower experimental magnetization.

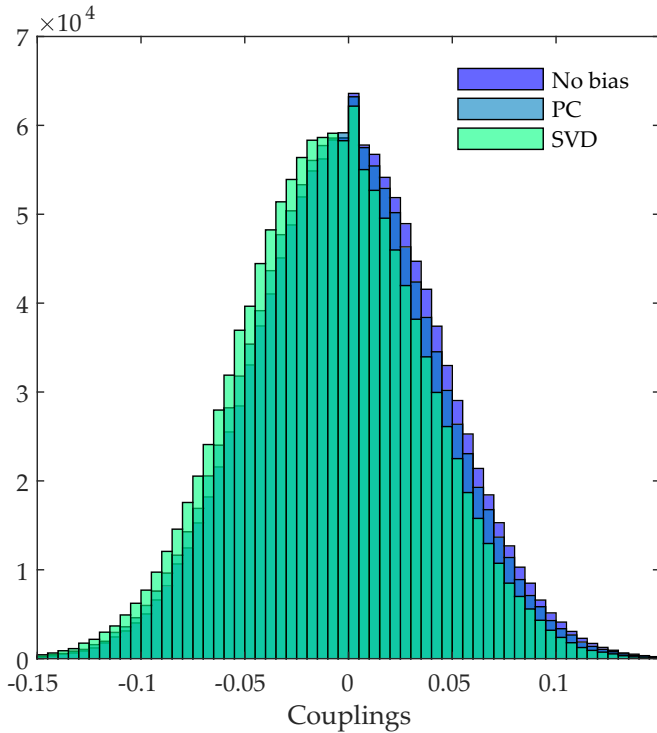


FIG. 7. Coupling distributions for systems with $M = N = 256$. In the case of SVD, the distribution results are more shifted than when using PC. This is in agreement with what is observed in Fig. 3 of the main text in terms of magnetization of the ground state.

complex element that has a magnitude of 1 and an argument equal to the opposite of that specific element in the initial transmission matrix; that is, if θ is the argument of an element in the TM, then $-\theta$ is the argument of the corresponding conjugated matrix.

For several output modes, one first needs to sum over the rows of the initial TM and then extract the arguments. Indeed, we control only N degrees of freedom thanks to the SLM,

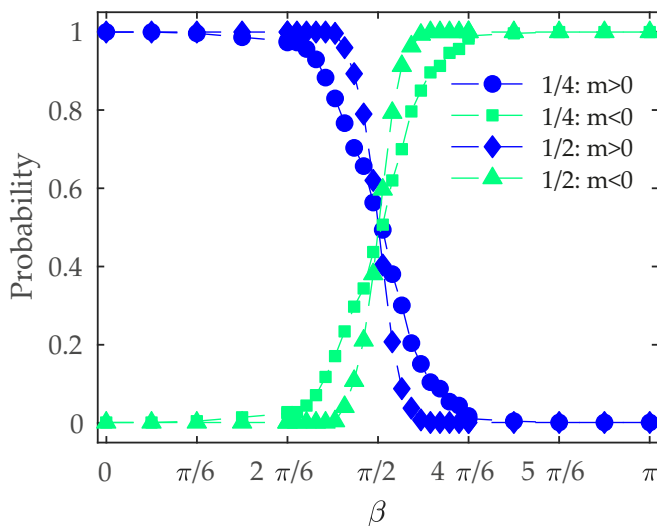


FIG. 8. Allocating a larger area of the SLM to the magnetic field results in a sharper phase transition.

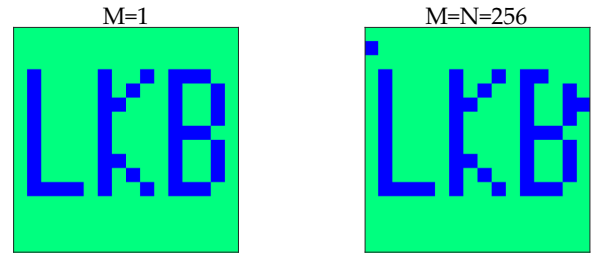


FIG. 9. Modifying the energy landscape to control the ground state of an Ising simulator. Examples show the spin ground state obtained using an additional binary bias showing the initials of Laboratory Kastler-Brossel.

but for several output modes the TM is $N \times m$. Once this is done, we can actually use the opposite angle to counteract the disorder medium. The larger the matrix is, the harder it is to actually get a proper focus.

The second method is based on the singular value decomposition (SVD). It is defined as follows: any given matrix $A \in \mathbb{C}$ of dimensions $m \times n$ can be factorized as $U \Sigma V^\dagger = A$, where the columns of U (V) represent the left (right) singular vectors, and the diagonal matrix Σ represents the singular values ranked by descending order; that is, the most representative vectors of A are the first ones in each matrix. In this particular nomenclature, the matrix V (U) encodes for the output (input) modes. One can therefore use the opposite of the arguments of the first right singular vector (V here) to act as a phase-conjugation substitute. Indeed, the *first* singular vector is the one with the biggest singular value and therefore is the one that represents the most the actual matrix.

APPENDIX B: NUMERICAL DETAILS

The numerical model used in this work is a generalization of what was described in [32]. The optical spin glass (SG) is numerically simulated by forming N pixel blocks (the SLM plane). The initial optical field has a constant amplitude, and its phase is a random configuration of N binary phases, $\phi_i = 0, \pi$. A transmission matrix T with random complex numbers is generated. At each iteration, a randomly selected single spin is flipped. The input phase updates if the output total intensity increased after the linear propagation of the field. The bias in the numerical framework is calculated as in the experiment by starting from the knowledge of T .

Numerical evaluation of I_T corresponds to a measurement with a detector in a noiseless system. In general, within this scheme, $\sim 10N$ iterations are sufficient for good convergence, i.e., when focus intensity reaches a plateau. All codes were implemented in MATLAB on an Intel processor with 14 cores running at 3.7 GHz and supported by 64 GB of RAM.

APPENDIX C: DETAILS OF THE ANALYTICAL CALCULATIONS

1. Noise bias

In addition to the context of having the spins superimposed with the SVD-retrieved angles to compensate for the medium,

one can define a random mask superimposed on top of this which reads $e^{i\theta\eta}$, where θ is a random value in $[0, 2\pi]$ and $\eta \in [0, 1]$ is a global parameter which defines how strong this noise is compared to the SVD angles ($\eta = 1$ means the noise is strong and therefore the situation is equivalent to not having retrieved any angles at all). Consequently, the intensity of one output mode m reads

$$\begin{aligned} I_T &= \left| \sum_i t_{im} E_i \right|^2 = \left(\sum_j \overline{t_{jm} E_j} \right) \left(\sum_i t_{im} E_i \right) \\ &= \sum_{i,j} t_{im} \overline{t_{jm} E_j} = \frac{1}{2} \left(2 \sum_{i,j} t_{im} \overline{t_{jm} E_j} \right), \end{aligned}$$

where $t_{im} = A_i e^{-i\tilde{\psi}_i}$ are the TM coefficients and $E_i = e^{i\phi_i} e^{i\psi_i} e^{i\eta\theta_i}$. The intensity and resulting couplings can therefore be rewritten as

$$I_T = \sum_{i,j} J_{ij} \tilde{\sigma}_i \sigma_j, \quad (\text{C1})$$

$$\tilde{J}_{ij} = -\text{Re}\{t_{im} e^{i\psi_i} e^{i\eta\theta_i} \overline{t_{jm} e^{-i\psi_j} e^{-i\eta\theta_j}}\}. \quad (\text{C2})$$

2. External magnetic field

To derive the effective external field, one needs to separate the SLM into two parts: one portion encodes for the spins, optimized by the algorithm, and one portion encodes for the external field, fixed during optimization. Therefore, considering the case where half the SLM is allocated to the spins $\sigma_i = e^{i\phi_i}$ as well as to the external field $h_j = e^{i\beta_j}$, one can divide the usual sum into two terms:

$$\begin{aligned} I_T &= \left| \sum_i t_{im} E_i \right|^2 \\ &= \left(\sum_{j=1}^{N/2} \overline{t_{jm} E_j} + \sum_{j=N/2+1}^N \overline{t_{jm} E_j} \right) \\ &\quad \times \left(\sum_{i=1}^{N/2} t_{im} E_i + \sum_{i=N/2+1}^N t_{im} E_i \right) \\ &= \sum_{i,j} \overline{t_{jm} t_{im} E_j} E_i + \sum_{i,j} \overline{t_{jm} t_{im} E_j} E_i \\ &\quad + \sum_{j=1}^{N/2} \sum_{i=N/2+1}^N \overline{t_{jm} t_{im} E_j} E_i + \sum_{i=1}^{N/2} \sum_{j=N/2+1}^N \overline{t_{jm} t_{im} E_j} E_i, \end{aligned}$$

where $E_i = e^{\phi_i + \psi_i}$ or $e^{\beta_i + \psi_i}$, depending on whether it corresponds to the spin area or the field area, respectively.

The first term is the one derived earlier which represents the classical Hamiltonian. The second one is simply a constant term based on the field value, which will not change during optimization and will be neglected in the coming equations. Acting on the index order, we obtain

$$\begin{aligned} I_T &= \sum_{i,j} J_{ij} \sigma_i \sigma_j + \sum_{j=1}^{N/2} \sum_{i=N/2+1}^N \overline{t_{jm} t_{im} E_j} E_i \\ &\quad + \sum_{i=1}^{N/2} \sum_{j=N/2+1}^N \overline{t_{jm} t_{im} E_j} E_i \end{aligned}$$

$$\begin{aligned} &= -H(\sigma) + \sum_{i=1}^{N/2} \sum_{j=N/2+1}^N (\overline{t_{jm} t_{im} E_j} E_i + \overline{t_{im} t_{jm} E_i} E_j) \\ &= -H(\sigma) + \sum_{i=1}^{N/2} \sum_{j=N/2+1}^N (\overline{t_{jm} t_{im} h_j} e^{-i\psi_j} \sigma_i e^{i\psi_i} \\ &\quad + \overline{t_{im} t_{jm} h_j} e^{i\psi_j} \overline{\sigma_i} e^{-i\psi_i}) \end{aligned}$$

By definition, $\sigma_i = e^{i\phi_i}$, and since the spins are binary ($\phi_i = 0, \pi$), $\sigma_i = 1, -1$, and therefore, $\overline{\sigma_i} = -\sigma_i$. Writing out the TM coefficients as $t_{im} = A_i e^{i\tilde{\psi}_i}$ and the field as $h_j = e^{i\beta_j}$, we get

$$\begin{aligned} I_T &= -H(\sigma) \\ &\quad + \sum_{i=1}^{N/2} \sum_{j=N/2+1}^N (A_j e^{i\tilde{\psi}_j} A_i e^{-i\tilde{\psi}_i} e^{-i\beta_j} e^{-i\psi_j} e^{i\psi_i} \sigma_i \\ &\quad + A_j e^{-i\tilde{\psi}_j} A_i e^{i\tilde{\psi}_i} e^{i\beta_j} e^{i\psi_j} e^{-i\psi_i} \overline{\sigma_i}) \\ &= -H(\sigma) \\ &\quad + \underbrace{\sum_{i=1}^{N/2} \sum_{j=N/2+1}^N \text{Re}\{e^{-i(\psi_j - \tilde{\psi}_j)} e^{i(\psi_i - \tilde{\psi}_i)} e^{i\beta_j}\} A_i A_j \sigma_i}_{(*)}. \end{aligned}$$

Now, $\psi_{i,j}$ are, by definition, the phase-conjugated angles of the TM, which implies that in the case of an ideal phase conjugation $\psi_i = \tilde{\psi}_i$. Considering the field is uniform, meaning $\beta_j = \beta$, this last term can therefore be rewritten as

$$\begin{aligned} (*) &= 2 \sum_i \sum_j \text{Re}\{e^{i\beta_j}\} A_i A_j \sigma_i \\ &= 2 \text{Re}\{e^{i\beta}\} \sum_j A_j \sum_i A_i \sigma_i \\ &= 2 \text{Re}\{e^{i\beta}\} \left(\sum_j A_j \right) \sum_i A_i \sigma_i. \end{aligned}$$

We therefore obtain

$$I_T = \sum_{i,j} J_{ij} \sigma_i \sigma_j + B \sum_i A_i \sigma_i,$$

where $B = 2 \text{Re}\{e^{i\beta}\} \sum_j A_j$ describes the effective external field.

APPENDIX D: ADDITIONAL FIGURES

The figures in this Appendix expand on the discussion in the main text. Figure 5 shows magnetization values for different experimental realizations and a comparison of different focus intensities. Figure 6 shows the expected magnetization as a function of the number of output modes and TM amplitudes associated with the SLM spins for $M = 256$. Figure 7 illustrates coupling distributions for systems with $M = N = 256$. Figure 8 shows what happens when a larger area of the SLM is allocated to the magnetic field. Finally, the modification of the energy landscape to control the ground state of an Ising simulator is illustrated in Fig. 9.

- [1] M. R. Garey and D. S. Johnson, *Computers and Intractability; A Guide to the Theory of NP-Completeness* (Freeman, New York, 1990).
- [2] S. Aaronson, *SIGACT News* **36**, 30 (2005).
- [3] F. Barahona, *J. Phys. A* **15**, 3241 (1982).
- [4] C. P. Bachas, *J. Phys. A* **17**, L709 (1984).
- [5] N. Nishimori, *Statistical Physics of Spin Glasses and Information Processing: An Introduction* (Clarendon, Oxford, 2001).
- [6] A. Lucas, *Front. Phys.* **2**, 5 (2014).
- [7] Y. Fu and P. Anderson, *J. Phys. A* **19**, 1605 (1986).
- [8] M. W. Johnson *et al.*, *Nature (London)* **473**, 194 (2011).
- [9] S. Boixo, T. F. Rønnow, S. V. Isakov, Z. Wang, D. Wecker, D. A. Lidar, J. M. Martinis, and M. Troyer, *Nat. Phys.* **10**, 218 (2014).
- [10] F. Tommasi, E. Ignesti, S. Lepri, and S. Cavalieri, *Sci. Rep.* **6**, 37113 (2016).
- [11] N. Ghofraniha, I. Viola, F. Di Maria, G. Barbarella, G. Gigli, L. Leuzzi, and C. Conti, *Nat. Commun.* **6**, 6058 (2015).
- [12] R. Harris *et al.*, *Science* **361**, 162 (2018).
- [13] R. Hamerly *et al.*, *Sci. Adv.* **5**, 0823 (2019).
- [14] N. G. Berloff, M. Silva, K. Kalinin, A. Askitopoulos, J. D. Töpfer, P. Cilibrizzi, W. Langbein, and P. G. Lagoudakis, *Nat. Mater.* **16**, 1120 (2017).
- [15] K. P. Kalinin, A. Amo, J. Bloch, and N. G. Berloff, *Nanophotonics* **9**, 4127 (2020).
- [16] D. Pierangeli, A. Tavani, F. Di Mei, A. J. Agranat, C. Conti, and E. DelRe, *Nat. Commun.* **8**, 1501 (2017).
- [17] T. Inagaki, K. Inaba, R. Hamerly, K. Inoue, Y. Yamamoto, and H. Takesue, *Nat. Photonics* **10**, 415 (2016).
- [18] A. Marandi, Z. Wang, K. Takata, R. L. Byer, and Y. Yamamoto, *Nat. Photonics* **8**, 937 (2014).
- [19] Y. Haribara, S. Utsunomiya, and Y. Yamamoto, in *Principles and Methods of Quantum Information Technologies*, Lecture Notes in Physics, Vol. 911, edited by Y. Yamamoto and K. Semba (Springer, Tokyo, 2016), pp. 251–262.
- [20] P. L. McMahon, A. Marandi, Y. Haribara, R. Hamerly, C. Langrock, S. Tamate, T. Inagaki, H. Takesue, S. Utsunomiya, K. Aihara, R. L. Byer, M. M. Fejer, H. Mabuchi, and Y. Yamamoto, *Science* **354**, 614 (2016).
- [21] T. Inagaki, Y. Haribara, K. Igarashi, T. Sonobe, S. Tamate, T. Honjo, A. Marandi, P. L. McMahon, T. Umeki, K. Enbutsu, O. Tadanaga, H. Takenouchi, K. Aihara, K. Kawarabayashi, K. Inoue, S. Utsunomiya, and H. Takesue, *Science* **354**, 603 (2016).
- [22] F. Böhm, G. Verschaffelt, and G. Van der Sande, *Nat. Commun.* **10**, 3538 (2019).
- [23] H. Takesue, K. Inaba, T. Inagaki, T. Ikuta, Y. Yamada, T. Honjo, T. Kazama, K. Enbutsu, T. Umeki, and R. Kasahara, *Phys. Rev. Appl.* **13**, 054059 (2020).
- [24] T. Honjo, T. Sonobe, K. Inaba, T. Inagaki, T. Ikuta, Y. Yamada, T. Kazama, K. Enbutsu, T. Umeki, R. Kasahara, K. Kawarabayashi, and H. Takesue, *Sci. Adv.* **7**, 0952 (2021).
- [25] M. Nixon, E. Ronen, A. A. Friesem, and N. Davidson, *Phys. Rev. Lett.* **110**, 184102 (2013).
- [26] R. Hamerly, T. Inagaki, P. L. McMahon, D. Venturelli, A. Marandi, D. R. Englund, and Y. Yamamoto, *Proc. SPIE* **11299**, 112990J (2020).
- [27] M. Calvanese Strinati, L. Bello, E. G. Dalla Torre, and A. Pe'er, *Phys. Rev. Lett.* **126**, 143901 (2021).
- [28] I. Gershenzon, G. Arwas, S. Gadas, C. Tradonsky, A. Friesem, O. Raz, and N. Davidson, *Nanophotonics* **9**, 4117 (2020).
- [29] H. Edri, B. Raz, G. Fleurov, R. Ozeri, and N. Davidson, *New J. Phys.* **23**, 053005 (2021).
- [30] D. Pierangeli, G. Marcucci, and C. Conti, *Phys. Rev. Lett.* **122**, 213902 (2019).
- [31] D. Pierangeli, G. Marcucci, and C. Conti, *Optica* **7**, 1535 (2020).
- [32] D. Pierangeli, M. Rafayelyan, C. Conti, and S. Gigan, *Phys. Rev. Appl.* **15**, 034087 (2021).
- [33] D. Pierangeli, G. Marcucci, D. Brunner, and C. Conti, *Nanophotonics* **9**, 4109 (2020).
- [34] M. Leonetti, E. Hörmann, L. Leuzzi, G. Parisi, and G. Ruocco, *Proc. Natl. Acad. Sci. USA* **118**, e2015207118 (2021).
- [35] Y. Fang, J. Huang, and Z. Ruan, *Phys. Rev. Lett.* **127**, 043902 (2021).
- [36] J. Huang, Y. Fang, and Z. Ruan, *Commun. Phys.* **4**, 242 (2021).
- [37] D. Mattis, *Phys. Lett. A* **56**, 421 (1976).
- [38] M. Mezard, G. Parisi, and M. Virasoro, *Spin Glass Theory and Beyond* (World Scientific, Singapore, 1986).
- [39] G. Parisi, *Statistical Field Theory* (Addison-Wesley, Redwood City, CA, 1988).
- [40] S. M. Popoff, G. Lerosey, R. Carminati, M. Fink, A. C. Boccara, and S. Gigan, *Phys. Rev. Lett.* **104**, 100601 (2010).
- [41] S. Rotter and S. Gigan, *Rev. Mod. Phys.* **89**, 015005 (2017).
- [42] D. S. Fisher and P. A. Lee, *Phys. Rev. B* **23**, 6851 (1981).
- [43] M. Davy, Z. Shi, J. Park, C. Tian, and A. Z. Genack, *Nat. Commun.* **6**, 6893 (2015).
- [44] R. Sarma, A. G. Yamilov, S. Petrenko, Y. Bromberg, and H. Cao, *Phys. Rev. Lett.* **117**, 086803 (2016).
- [45] L. C. Hollenberg and M. J. Tomlinson, *Aust. J. Phys.* **47**, 137 (1994).
- [46] M. Nixon, O. Katz, E. Small, Y. Bromberg, A. A. Friesem, Y. Silberberg, and N. Davidson, *Nat. Photonics* **7**, 919 (2013).